State-of-Charge Estimation of the Lithium-Ion Battery Using an Adaptive Extended Kalman Filter Based on an Improved Thevenin Model

Hongwen He, Rui Xiong, Xiaowei Zhang, Fengchun Sun, and JinXin Fan, *Student Member, IEEE*

***Abstract*—An adaptive Kalman filter algorithm is adopted to estimate the state of charge (SOC) of a lithium-ion battery for application in electric vehicles (EVs). Generally, the Kalman filter algorithm is selected to dynamically estimate the SOC. However, it easily causes divergence due to the uncertainty of the battery model and system noise. To obtain a better convergent and robust result, an adaptive Kalman filter algorithm that can greatly improve the dependence of the traditional filter algorithm on the battery model is employed. In this paper, the typical characteristics of the lithium-ion battery are analyzed by experiment, such as hysteresis, polarization, Coulomb efficiency, etc. In addition, an improved Thevenin battery model is achieved by adding an extra RC branch to the Thevenin model, and model parameters are identified by using the extended Kalman filter (EKF) algorithm. Further, an adaptive EKF (AEKF) algorithm is adopted to the SOC estimation of the lithium-ion battery. Finally, the proposed method is evaluated by experiments with federal urban driving schedules. The proposed SOC estimation using AEKF is more accurate and reliable than that using EKF. The comparison shows that the maximum SOC estimation error decreases from 14.96% to 2.54% and that the mean SOC estimation error reduces from 3.19% to 1.06%.**

***Index Terms*—Adaptive extended Kalman filter (AEKF), battery model, electric vehicles (EVs), parameter identification, state of charge (SOC).**

I. Introduction

THE BATTERY pack, as a key component, is crucial for the performance of electric vehicles (EVs), such as economy, power performance, security, etc. It is significant to accurately manage the battery pack to extend its lifespan, improve its reliability, and lower its cost. The online state-of-charge (SOC) estimation of battery pack, which is also vital for the power distribution strategy of EVs [1]–[4], is one of the main tasks of the battery management system [4]–[7]. A number of methods to estimate the SOC have been proposed, each with its own advantages and disadvantages [8]–[17]. According to the choice of the battery model, some commonly used methods can approximately be categorized into three types. One type is the Coulomb counting method, which is an open-loop algorithm with the flaws of big accumulation of measurement errors due to uncertain disturbances and difficulty to determine the initial value of SOC accurately. The second type is based on black-box battery models that describe the nonlinear relationship between the SOC and its influencing factors, which can often produce a good estimate of the SOC due to the powerful ability to approximate nonlinear function surfaces, with the flaws of heavy computation burden and bad real-time application. The third type is based on state estimation techniques with state-space battery models, which is popular due to the advantages of being close-loop, online, and available to dynamically regulate the estimation error range.

The extended Kalman filter (EKF) algorithm can not only be used to implement the parameter identification of the battery model but also be employed for online SOC estimation [12]–[22]. In particular, it is suitable for dynamic driving conditions. However, it strongly depends on the accuracy of the battery model as well as the predetermined variables of the system noise, such as mean value, pertinence, and covariance matrix. Usually, the improper setting of the predetermined variables of the system noise may result in remarkable errors and divergence.

To obtain more accurate and robust SOC estimation, in this paper, an improved Thevenin battery model is put forward, which is based on the analysis of the polarization characteristics of a lithium-ion battery module by experimental results, and its parameters are identified by the EKF algorithm. In addition, an adaptive EKF (AEKF) algorithm is designed for the SOC estimation of the lithium-ion battery module.

II. Model and Parameter Identification of Lithium-Ion Battery Module

A. Lithium-Ion Battery Modeling

Generally, equivalent circuit models are selected, which include the Rint model, the Thevenin model, the RC model, and the partnership for a new generation of vehicle (PNGV) model [15], [23]–[25], for battery modeling. Among them, the Thevenin model is widely used to model the lithium-ion battery, but it is still not accurate enough since all of its elements can change, depending on the condition and state of the battery. To improve the model accuracy, the polarization characteristics of the lithium-ion battery are particularly considered, and an

Manuscript received September 19, 2010; revised January 16, 2011; accepted March 13, 2011. Date of publication March 28, 2011; date of current version May 16, 2011. This work was supported in part by the National High Technology Research and Development Program of China under Grant 2008AA11A124. The review of this paper was coordinated by Dr. R. Langari.

The authors are with the National Engineering Laboratory for Electric Vehicles, School of Mechanical Engineering, Beijing Institute of Technology, Beijing 100081, China (e-mail: hwhebit@bit.edu.cn; xrui_ev@126.com; fot8150@bit.edu.cn; sunfch@bit.edu.cn; jinxinfan@gmail.com).

Color versions of one or more of the figures in this paper are available online at http://ieeexplore.ieee.org.

Digital Object Identifier 10.1109/TVT.2011.2132812

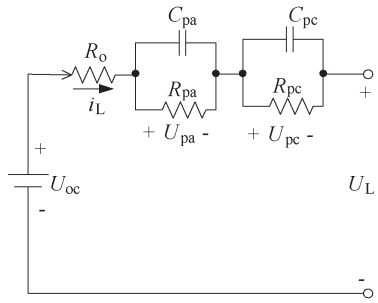

Fig. 1. Schematic of the improved Thevenin model.

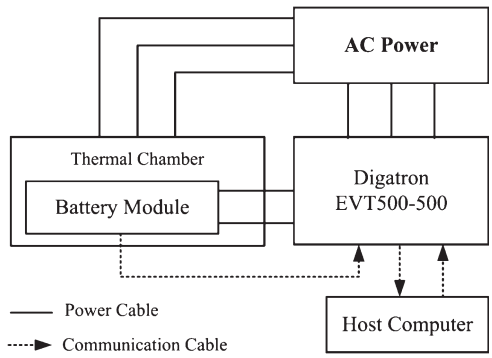

Fig. 2. Configuration of the battery test bench.

improved Thevenin model, which is performed by adding an extra RC branch to the Thevenin model, as shown in Fig. 1, is proposed accordingly.

The improved Thevenin model includes three parts as open-circuit voltage $U_{\rm OC}$, internal resistances, and equivalent capacitances. The internal resistances include ohmic resistance R_O, electrochemical polarization resistance $R_{\rm pa}$, and concentration polarization resistance $R_{\rm pc}$. The equivalent capacitances, which include electrochemical polarization capacitance $C_{\rm pa}$ and concentration polarization capacitance $C_{\rm pc}$, are used to describe the transient response during the charging /discharging transits. i_L and U_L are the charging/discharging current and the terminal voltage, respectively. The electrical behavior of the circuit can be expressed as follows:

$$\begin{cases} \dot{U}_{\rm pa} = -U_{\rm pa}/(R_{\rm pa}C_{\rm pa}) + i_L/C_{\rm pa} \\ \dot{U}_{\rm pc} = -U_{\rm pc}/(R_{\rm pc}C_{\rm pc}) + i_L/C_{\rm pc} \\ U_L = U_{\rm OC} - U_{\rm pa} - U_{\rm pc} - i_L R_O \end{cases} \quad (1)$$

where $U_{\rm pa}$ and $U_{\rm pc}$ are the voltages on $C_{\rm pa}$ and $C_{\rm pc}$, respectively.

B. Experiments

To identify the parameters of the improved Thevenin model, the battery test bench is designed. Charging and discharging experiments are carried out on a lithium-ion battery module (from Chinese CITIC GUOAN MGL Company) with nominal voltage of 57.6 V and nominal capacity of 100 Ah.

1) Battery Test Bench: Fig. 2 shows the configuration of the battery test bench. Its key equipment is Digatron EVT500-500, which can charge or discharge the battery module with a maximum voltage of 500 V and a maximum current of 500 A and can timely measure the major parameters like voltage, current, and temperature. The host computer with the installed software BTS-600 can program the experiment procedure and deal with real-time data acquisition. To reduce the influence of temperature, the battery module being tested is kept in a thermal chamber.

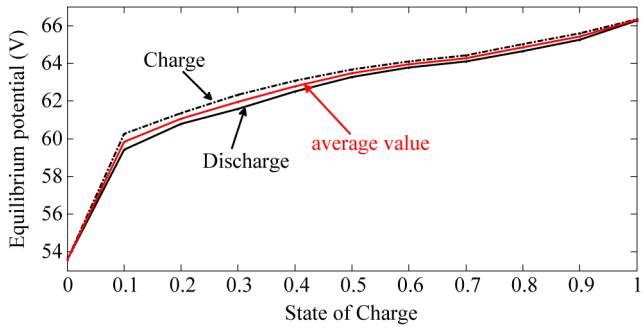

Fig. 3. Equilibrium potential and open-circuit voltage curves of the battery module.

2) Open-Circuit Voltage Identification Test: To acquire data to identify the parameters of the open-circuit voltage, a test was performed on the lithium-ion battery module. The test procedure is as follows: The battery module is first discharged at a constant current of 0.3C A from the fully charged state to 90% of the nominal capacity at 20 °C in the thermal chamber. Afterwards, it is left in the open-circuit condition, and the terminal voltage is monitored simultaneously. The measured terminal voltage is considered to reach the equilibrium potential after 10 h since the change of the terminal voltage is negligible and the battery module is assumed to reach steady state. The battery module is continuously discharged by a further 10% of the nominal capacity at the same current, and the equilibrium potential is measured after 10 h. The foregoing procedure was repeatedly performed to obtain the equilibrium potentials, shown as the discharge curve in Fig. 3. The equilibrium potentials on the charge curve in Fig. 3 were obtained with a similar test procedure by charging the battery pack at a constant current of 0.3C A from the fully discharged state with the step of 10% of the nominal capacity.

It can be found that the equilibrium potential has different values after charging and discharging, respectively, at the same SOC. The equilibrium potential is higher at the charging process than that at the discharging process, which indicates that the equilibrium potential depends on the previous treatment of the battery module, and hysteresis occurs during the charging/discharging. In this paper, the hysteresis is ignored, and the open-circuit voltage $U_{\rm OC}$ is defined as the average of the equilibrium potentials of charging and discharging to simplify the model.

The open-circuit voltage $U_{\rm OC}$ measured as a function of the SOC, which is shown as follows, can be obtained by curve fitting with the quadratic fitting method:

$$U_{\rm OC}({\rm SOC}) = -13 \times {\rm SOC}^2 + 22 \times {\rm SOC} + 57. \quad (2)$$

3) HPPC Test: To acquire data to identify the model parameters, a hybrid pulse power characterization (HPPC) test was conducted on the lithium-ion battery module at 10% SOC

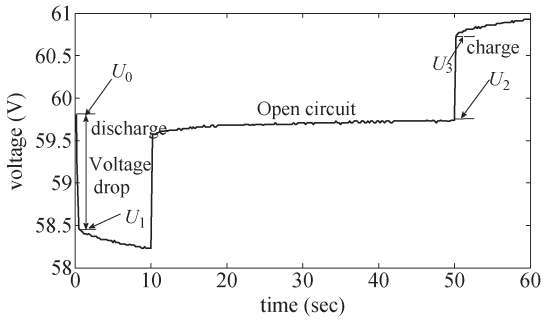

Fig. 4. Battery module voltage profile during HPPC test at SOC $= 0.1$.

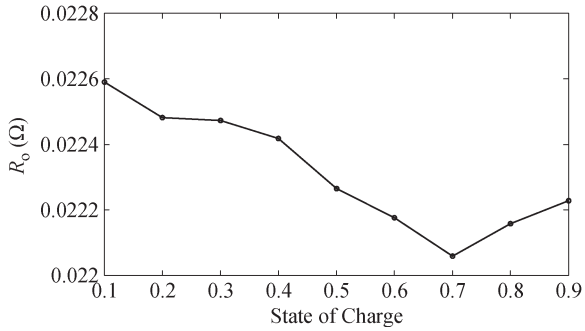

Fig. 5. Ohmic resistance characteristic curve of the battery module.

intervals starting from 0.9 to 0.1. During the test, the temperature of the battery module was kept at 20 °C in the thermal chamber. Fig. 4 shows the terminal voltage profile of the tested battery module during an HPPC test at SOC $= 0.1$.

As shown in Fig. 4, a voltage drop appears when a pulse discharge/charge current is loaded, which can be expressed as

$$\Delta U = \begin{cases} |U_1 - U_0|, & \text{when discharging} \\ |U_3 - U_2|, & \text{when charging.} \end{cases} \tag{3}$$

Then, the ohmic resistance R_O can be given by

$$R_O = \Delta U / |i_L|. \tag{4}$$

The ohmic resistance R_O is found to be independent of the battery load current and is a function of the SOC shown in Fig. 5.

C. Parameter Identification

1) EKF Algorithm: The Kalman filter is a set of mathematical equations that provide an efficient recursive means to estimate the state of a process in a way that minimizes the mean of the squared error. The filter has extensively been applied to the field of linear estimation, including state estimation, parameter estimation, and dual estimation. The EKF algorithm is a nonlinear version of the Kalman filter that linearizes about the current mean and covariance of the state. It can be described as follows for a continuous-time system with discrete-time measurements [12], [18]:

$$\begin{cases} \dot{\mathbf{x}} = f(\mathbf{x}, \mathbf{u}, \mathbf{w}, t) \\ \mathbf{y}_k = h(\mathbf{x}_k, \mathbf{v}_k) \\ \mathbf{w} \sim (0, \mathbf{Q}) \\ \mathbf{v}_k \sim (0, \mathbf{R}_k) \end{cases} \tag{5}$$

where $\mathbf{u}$ is the system input; $\mathbf{w}$ is the process noise and is a continuous-time Gaussian white noise with zero mean and covariance of $\mathbf{Q}$; and $\mathbf{v}_k$ is the measurement noise and is a discrete-time Gaussian white noise with zero mean and covariance of $\mathbf{R}_k$. The nonlinear function $h(\bullet)$ relates the state at the previous time step $k-1$ to the state at the current time step k.

The filter step for optimal state and parameter estimation can be summarized as follows.

Step I: Initialization: The initial estimation of $\mathbf{x}_0$ before any measurement is modeled as a Gaussian random vector with mean of $\mathbf{x}_0$ and covariance of $\mathbf{P}_0$, which is expressed by

$$\begin{cases} \hat{\mathbf{x}}_0^+ = E[\mathbf{x}_0] \\ \mathbf{P}_0^+ = E\left[\left(\mathbf{x}_0 - \hat{\mathbf{x}}_0^+\right)\left(\mathbf{x}_0 - \hat{\mathbf{x}}_0^+\right)^T\right]. \end{cases} \tag{6}$$

Step II: Time update (from time $(k-1)^+$ to time $(k)^-$): In this step, an estimate of the state at the current time step $(k)^-$ is produced based on the state estimate and its covariance from the previous time step $(k-1)^+$, i.e.,

$$\begin{aligned} \dot{\hat{\mathbf{x}}} &= f(\hat{\mathbf{x}}, \mathbf{u}, \mathbf{w}, t) \\ \dot{\mathbf{P}} &= \mathbf{AP} + \mathbf{PA^T} + \mathbf{Q}. \end{aligned} \tag{7}$$

$\mathbf{A}$ is the Jacobian matrix of partial derivatives of $f(\bullet)$ with respect to $\mathbf{x}$, i.e.,

$$\mathbf{A}_{[i,j]} = \left.\frac{\partial f_{[i]}}{\partial \mathbf{x}_{[j]}}\right|_{x=\hat{x}}. \tag{8}$$

In this step, the integration is processed with $\hat{\mathbf{x}}_k = \hat{\mathbf{x}}_{k-1}^+$ and $\mathbf{P}_k = \mathbf{P}_{k-1}^+$. At the end of the integration, we have $\hat{\mathbf{x}}_k = \hat{\mathbf{x}}_k^-$ and $\mathbf{P}_k = \mathbf{P}_k^-$. With reference to (7), the estimate state and its covariance propagates from time $(k-1)^+$ to time $(k)^-$ based on the previous values, the system dynamic, the control input, and the errors of the actual system.

Step III: Measurement update: In this step, the measurement information at time k is processed to refine the estimate of $\mathbf{x}_k$ to reach a more accurate state estimate. In addition, the observed vector $\mathbf{y}_k$ is used to correct the state estimation and the covariance estimation. The resulting estimate of $\mathbf{x}_k$ is denoted as $\hat{\mathbf{x}}_k^+$, and its covariance is denoted as $\mathbf{P}_k^+$. The measurement update of the state estimation and the estimation error covariance is performed according to the following equations:

$$\begin{cases} \mathbf{K}_k = \mathbf{P}_k^- \mathbf{C}_k^T \left(\mathbf{C}_k \mathbf{P}_k^- \mathbf{C}_k^T + \mathbf{R}_k\right)^{-1} \\ \hat{\mathbf{x}}_k^+ = \hat{\mathbf{x}}_k^- + \mathbf{K}_k \left(\mathbf{y}_k - h\left(\hat{\mathbf{x}}_k^-, \mathbf{v}_k\right)\right) \\ \mathbf{P}_k^+ = (\mathbf{I} - \mathbf{K}_k \mathbf{C}_k)\mathbf{P}_k^-(\mathbf{I} - \mathbf{K}_k \mathbf{C}_k)^T + \mathbf{K}_k \mathbf{R}_k \mathbf{K}_k^T \end{cases} \tag{9}$$

where $\mathbf{K}_k$ is the Kalman gain matrix, and $\mathbf{C}_k$ is the partial derivative of $h(\cdot)$ with respect $\mathbf{x}$, which is given by

$$\mathbf{C}_{[i,j]} = \frac{\partial h_{[i]}}{\partial \mathbf{x}_{[\mathrm{j}]}}\left(\hat{\mathbf{x}}_k^-, \mathbf{v}_k\right). \tag{10}$$

It should be noted that $\hat{\mathbf{x}}_k^-$ and $\hat{\mathbf{x}}_k^+$ are both estimations of the same vector $\mathbf{x}_k$. However, $\hat{\mathbf{x}}_k^-$ is the estimate of $\mathbf{x}_k$ before the measurement $\mathbf{y}_k$ is taken into account, which is called the *a priori* estimate, and $\hat{\mathbf{x}}_k^+$ is the estimate of $\mathbf{x}_k$ after the

measurement $\mathbf{y}_k$ is considered, which is called the *a posteriori* estimate [18].

2) Parameter Identification With EKF: This section presents the implementation of EKF for estimating the states and parameters of the improved battery model.

The terminal voltage U_L can be rearranged based on (1) as

$$U_L = U_{\rm OC} + [-1 \quad -1]\begin{bmatrix} U_{\rm pa} \\ U_{\rm pc} \end{bmatrix} - [R_O] i_L. \tag{11}$$

On the assumption that $dU_{\rm OC}/dt \approx 0$, taking time the derivative of U_L gives

$$\dot{U}_L = \left[-\frac{1}{R_{\rm pc}C_{\rm pc}}\right] U_L + \left[\frac{1}{R_{\rm pa}C_{\rm pa}} - \frac{1}{R_{\rm pc}C_{\rm pc}}\right] U_{\rm pa} - \left[\frac{R_O}{R_{\rm pc}C_{\rm pc}} + \frac{1}{C_{\rm pc}} + \frac{1}{C_{\rm pa}}\right] i_L + \left[\frac{1}{R_{\rm pc}C_{\rm pc}}\right] U_{\rm OC}. \tag{12}$$

Transform (12) into the form of (5) as

$$f(\mathbf{x}, \mathbf{u}) = [f_1 \quad f_2 \quad f_3 \quad f_4 \quad f_5 \quad f_6 \quad f_7]^{\mathbf{T}} \tag{13}$$

$$\mathbf{y}_k = h(\mathbf{x}_k) = [0 \quad 0 \quad U_{\rm Lk} \quad 0 \quad 0 \quad 0 \quad 0]^{\mathbf{T}} \tag{14}$$

where f_i $(i = 1, 2, 3, 4, 5, 6, 7)$ and $\mathbf{x}$ are defined as follows:

$$\begin{cases} \mathbf{x} = [U_{\rm pa} \quad U_{\rm pc} \quad U_L \quad 1/R_{\rm pa} \quad 1/C_{\rm pa} \quad 1/R_{\rm pc} \quad 1/C_{\rm pc}]^{\mathbf{T}} \\ u = i_L \\ f_1 = -x_1x_4x_5 + x_5u \\ f_2 = -x_2x_6x_7 + x_7u \\ f_3 = -x_6x_7x_3 + (x_4x_5 - x_6x_7)x_1 \\ \qquad -(R_Ox_6x_7 + x_5 + x_7)u + x_6x_7U_{\rm OC} \\ f_4 = f_5 = f_6 = f_7 = 0. \end{cases} \tag{15}$$

The system matrix $\mathbf{A}$ is calculated as

$$\mathbf{A} = \left.\frac{\partial f}{\partial \mathbf{x}}\right|_{\mathbf{x}=\hat{\mathbf{x}}} = \begin{bmatrix} a_{11} & 0 & 0 & a_{14} & a_{15} & 0 & 0 \\ 0 & a_{22} & 0 & 0 & 0 & a_{26} & a_{27} \\ a_{31} & 0 & a_{33} & a_{34} & a_{35} & a_{36} & a_{37} \\ 0 & 0 & 0 & 0 & 0 & 0 & 0 \\ 0 & 0 & 0 & 0 & 0 & 0 & 0 \\ 0 & 0 & 0 & 0 & 0 & 0 & 0 \\ 0 & 0 & 0 & 0 & 0 & 0 & 0 \end{bmatrix} \tag{16}$$

where in matrix $\mathbf{A}$, $a_{11} = -x_4x_5$, $a_{14} = -x_1x_5$, $a_{15} = -x_1x_4 + u$, $a_{22} = -x_6x_7$, $a_{26} = -x_2x_7$, $a_{27} = -x_2x_6 + u$, $a_{31} = x_4x_5 - x_6x_7$, $a_{33} = -x_6x_7$, $a_{34} = x_5x_1$, $a_{35} = x_4x_1 - u$, $a_{36} = -x_7x_3 - x_7x_1 - R_Ox_7u + U_{\rm OC}x_7$, and $a_{37} = -x_6x_3 - x_6x_1 - R_Ox_6u - u + U_{\rm OC}x_6$.

The observe matrix $\mathbf{C}$ can be derived from (14) as

$$\mathbf{C} = [0 \quad 0 \quad 1 \quad 0 \quad 0 \quad 0 \quad 0]. \tag{17}$$

The identification results of the battery model parameters with EKF are shown in Fig. 6.

The estimation of polarization voltages as a function of time is shown in Fig. 6(a) and (b), respectively. In Fig. 6(a), it can be found that the voltage of the battery activation polarization reaches steady state within 0.2 s, which indicates that the time constant of the activation polarization RC branch is small. However, it takes a much longer time for the voltage of the battery concentration polarization to obtain steady state, as shown in Fig. 6(b). The curves of polarization resistances and polarization capacitors with time are shown in Figs. 6(c)–(f), respectively, which indicate that the estimated parameters quickly converge and keep constant within 60 s. It is verified that the parameter identification using the EKF algorithm is stable. Fig. 6(g) shows that the identification error is small and demonstrates good agreement between the results obtained using the voltage model-based EKF estimation and experiments.

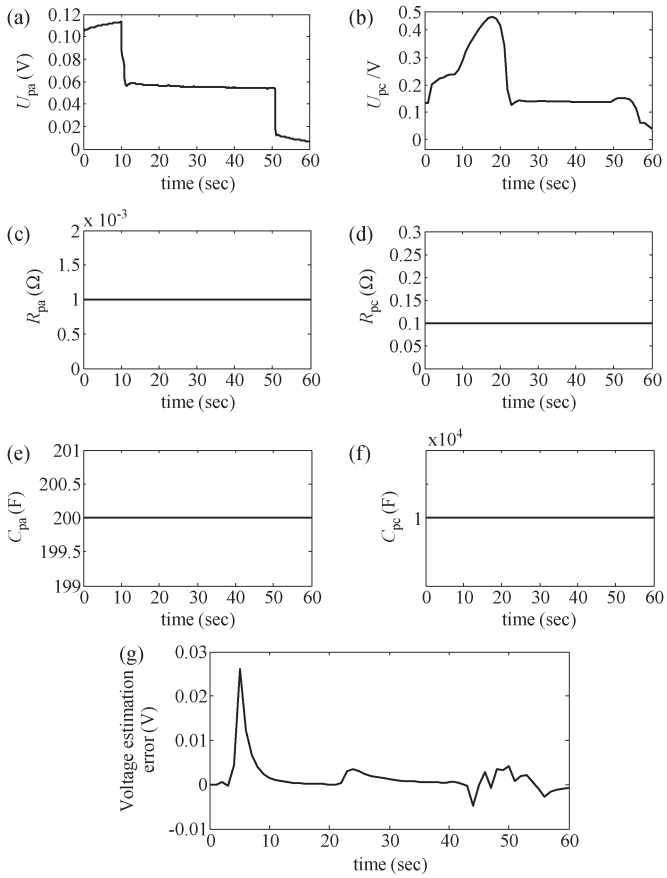

Fig. 6. Estimation results of the battery model parameters with EKF (SOC = 0.1).

TABLE I
MODEL PARAMETER LIST IDENTIFIED OF THE BATTERY MODULE

SOC	0.1	0.2	0.3	0.4	0.5
$R_{\rm pa}$ (Ω)	0.001	0.001	0.001	0.001	0.001
$C_{\rm pa}$ (F)	200.01	200	199.99	202	202. 2
$R_{\rm pc}$ (Ω)	0.1	0.1	0.0987	0.099	0.0994
$C_{\rm pc}$ (F)	10000	10000	9909	10010	10009
SOC	0.6	0.7	0.8	0.9	1.0
$R_{\rm pa}$ (Ω)	0.001	0.001	0.001	0.001	0.001
$C_{\rm pa}$ (F)	204.2	201.1	200.2	200.1	200.5
$R_{\rm pc}$ (Ω)	0.097	0.0941	0.0996	0.0999	0.1025
$C_{\rm pc}$ (F)	9903	9921	10210	9666	9987

Table I shows the identification results within the SOC range from 0.1 to 1.0.

D. Model Verification

To evaluate the validity of the improved Thevenin model, a testing cycle of HPPC shown in Fig. 7 is adopted as the input

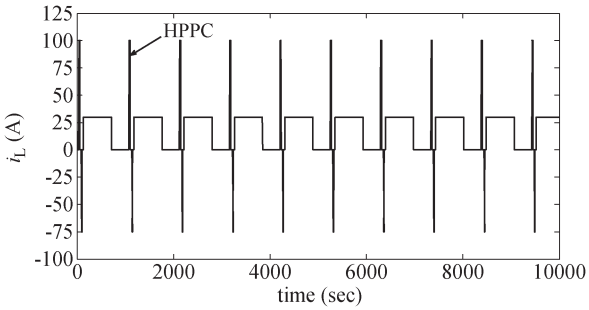

Fig. 7. Testing cycle for evaluating the validity of the battery module model.

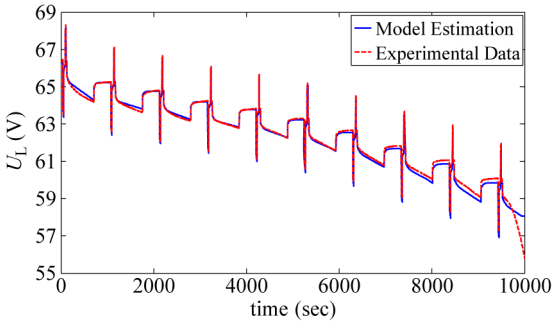

Fig. 8. Comparison between voltage response of the model and the experiment.

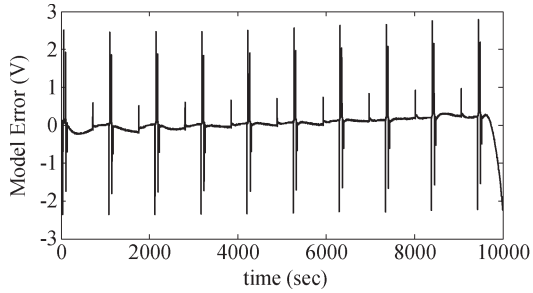

Fig. 9. Voltage error curves between simulation and experimental data.

TABLE II
STATISTIC LIST OF VOLTAGE ERRORS

Index	Maximum	Mean	Variance	Error rate
Value	2.79V	0.0337V	0.0708V^2	4.15%

for both the lithium-ion battery module and the battery module model. The initial SOC is 1.0. The parameters of the battery module model as a function of SOC are updated via linear lookup table and extrapolation. Fig. 8 presents the comparison of the experimental data with the model simulation data, which clearly shows the coincidence of two cases. (The i_L is positive in the discharging process and negative in the charging process.)

Fig. 9 shows the voltage error curves between the simulation data and the experimental data. Table II gives the statistic result of the voltage errors.

Table II shows that the error variance is 0.0708 V^2 and the error mean is around 0.0337 V, and the maximum error rate is 4.15%, which verifies that the parameter identification algorithm and the improved Thevenin model are accurate and reasonable. The errors are higher in Fig. 9 than the results shown in Fig. 6(g) because the SOC range is from 1.0 to 0.1, whereas that in Fig. 6(g) is only for a single SOC point.

TABLE III
COULOMBIC EFFICIENCY LIST OF THE LITHIUM-ION BATTERY MODULE

Current (A)	C/3	0.5C	1C	1.5C	2C	3C
Discharging coulombic efficiency (%)	100	99.3	98.5	98.05	97.4	95.16
Charging coulombic efficiency (%)	100	98.5	97.4	96.0	94.0	-

III. STATE-OF-CHARGE ESTIMATION USING THE ADAPTIVE EXTENDED KALMAN FILTER

A. SOC Definition

SOC is a relative quantity that describes the ratio of the remaining capacity to the nominal capacity of a battery. It is given by

$$\mathrm{SOC} = \mathrm{SOC}_0 - \frac{\int \eta i_L dt}{C_N} \tag{18}$$

where SOC_0 is the initial value of the SOC, η is the Coulombic efficiency, and C_N is the nominal capacity.

Transform (18) to discrete form, and use s as the abbreviation of SOC, i.e.,

$$s_k = s_{k-1} - \eta i_{L,k-1} \Delta t / C_N \tag{19}$$

where Δt is the discrete time step, s_k and s_{k-1} are the SOC values at k and $k-1$ step, and $i_{L,k-1}$ is the bus current at $k-1$ step.

Due to the polarization of the battery module, power losses obviously occur in the charging/discharging process, and the Coulombic efficiency consequently needs to be considered. The experimental data of the Coulombic efficiency under different charging/discharging currents for the lithium-ion battery module are shown in Table III.

B. SOC Estimation

1) AEKF: When using the Kalman filter to implement SOC estimation, although sometimes the estimation error covariance matrix continues to decrease, the actual error may still be larger than its theoretically value, and the actual error will extend constantly with the data increase; this phenomenon is often defined as divergence. Divergence will cause failures in the Kalman filter and will at least decrease its accuracy. One purpose of the adaptive filter is to judge whether the dynamic of the target has changed during doing recursive filter based on measurement data. If yes, then the adaptive filter must further decide whether to treat this change as a random noise and classify them to the model noise or to modify the primary model so that it could adapt the dynamic of the target. Another purpose of the adaptive filter is to estimate and modify the statistics of the noise or gain matrix of the filter continuously employing the information brought by observation data to improve the accuracy of the filter when the system noise variance and the observation noise variance are unknown [22]. The Sage–Husa

adaptive filter algorithm treats the target dynamic as a random disturbance and classifies it as a model noise; it is easy to be implemented and applied for time-varying systems with the defects of poor real-time calculation [26]. To overcome the drawback, we introduce a filter divergence judgment condition. If the filtering result exceeds the presetting divergence condition, then the noise estimator will be started to do adaptive filter calculating. Thus, it not only effectively avoids filter divergence and improves the stability of filter calculation but also improves the real-time ability of the filter.

The state and observation equations of the discrete system of interest is as follows:

$$\begin{cases} \mathbf{X}_k = \mathbf{A}_{k-1}\mathbf{X}_{k-1} + \mathbf{B}_{k-1}\mathbf{u}_{k-1} + \mathbf{\Gamma}_{k-1}\mathbf{w}_{k-1} \\ \mathbf{Y}_k = \mathbf{C}_k\mathbf{X}_k + \mathbf{D}_k\mathbf{u}_k + \mathbf{v}_k \\ \mathbf{v}_k \sim (\mathbf{r}_k, \mathbf{R}_k) \\ \mathbf{w}_k \sim (\mathbf{q}_k, \mathbf{Q}_k) \end{cases} \tag{20}$$

where $\mathbf{X}$ is an $n \times 1$ state vector; $\mathbf{Y}$ is an $m \times 1$ observe matrix; $\mathbf{A}$, $\mathbf{B}$, $\mathbf{C}$, $\mathbf{D}$, and Γ are $n \times n$, $n \times 1$, $m \times n$, $m \times 1$, and $n \times n$ matrix, respectively; $\mathbf{w}_k$ is the process noise with mean of $\mathbf{q}_k$ and covariance of $\mathbf{Q}_k$; and $\mathbf{v}_k$ is measurement noise with mean of $\mathbf{r}_k$ and covariance of $\mathbf{R}_k$.

The statistical characteristics of the initial state $\mathbf{X}_0$ are the same as (6). Sage and Husa proposed the maximum posterior suboptimal unbiased estimator based on the noise statistics of the observer $\mathbf{Y}$, but the unbiased estimator they proposed is the arithmetic average, and the weighted coefficients of each item are $1/(k+1)$. For the time-varying noise, there should be more emphasis put on the role of the recent data. Many researchers have adopted the index weighted method [22], that is, using the index weighted coefficient to replace the simple coefficient $1/(k+1)$.

The index weighted coefficient β_k is usually designed as

$$\beta_i = \beta_{i-1}b, 0 < b < 1, \quad \sum_{t=0}^{k} \beta_i = 1. \tag{21}$$

As an example, the following equation gives the calculation method of β_k:

$$\beta_i = d_k b, d_k = (1-b)/(1-b^{k+1}) \quad (i = 0, 1, 2, \ldots, k) \tag{22}$$

where b is a forgetting factor.

The improved noise estimator is recalculated as follows by replacing the weighted coefficient $1/(k+1)$ with the new weighted coefficient β_{k-1}:

$$\hat{\mathbf{q}}_{k+1} = (1-d_k)\hat{\mathbf{q}}_k + d_k \left\{ \mathbf{G}_k \sum_{i=0}^{k} [\hat{\mathbf{X}}_{k+1} - \mathbf{A}_k\hat{\mathbf{X}}_k - \mathbf{B}_k\mathbf{u}_k] \right\} \tag{23}$$

$$\begin{aligned} \hat{\mathbf{Q}}_{k+1} = {} & (1-d_k)\hat{\mathbf{Q}}_k \\ & + d_k \left\{ \mathbf{G}_k \left(\sum_{i=0}^{k} \left[\mathbf{K}_{k+1}\tilde{\mathbf{Y}}_{k+1}\tilde{\mathbf{Y}}_{k+1}^T\mathbf{K}_{k+1}^T \right. \right. \right. \\ & \left. \left. \left. + \mathbf{P}_{k+1} - \mathbf{A}_k\mathbf{P}_k\mathbf{A}_k^T \right] \right) \mathbf{G}_k^T \right\} \end{aligned} \tag{24}$$

$$\hat{\mathbf{r}}_{k+1} = (1-d_k)\hat{\mathbf{r}}_k + d_k \left\{ \sum_{i=0}^{k} \left[\mathbf{Y}_{k+1} - \mathbf{C}_k\hat{\mathbf{X}}_{k+1}^- - \mathbf{D}_k\mathbf{u}_k \right] \right\} \tag{25}$$

$$\begin{aligned} \hat{\mathbf{R}}_{k+1} = {} & (1-d_k)\hat{\mathbf{R}}_k \\ & + d_k \left\{ \sum_{i=0}^{k} \left[\tilde{\mathbf{Y}}_{k+1}\tilde{\mathbf{Y}}_{k+1}^T - \mathbf{C}_{k+1}\mathbf{P}_{k+1}^-\mathbf{C}_{k+1}^T \right] \right\} \end{aligned} \tag{26}$$

where $\mathbf{G}_k = [\mathbf{\Gamma}_k^T\mathbf{\Gamma}_k^-]^{-1}\mathbf{\Gamma}_k^T$; error matrix $\tilde{\mathbf{Y}}_{k+1} = \mathbf{Y}_{k+1} - \mathbf{C}_{k+1}(\mathbf{A}_{k+1}\hat{\mathbf{X}}_{k+1}^- + \mathbf{B}_{k+1}\mathbf{u}_{k+1}) - \mathbf{D}_{k+1}\mathbf{u}_{k+1} - \hat{\boldsymbol{r}}_k$; gain matrix $\mathbf{K}_{k+1} = \mathbf{P}_{k+1}^-\mathbf{C}_{k+1}^T[C_{k+1}\mathbf{P}_{k+1}^-\mathbf{C}_{k+1}^T + \hat{\mathbf{R}}_k]^{-1}$; and estimate of the covariance $\mathbf{P}_{k+1}^- = \mathbf{A}_k\mathbf{P}_k\mathbf{A}_k^T + \mathbf{\Gamma}_k\hat{\mathbf{Q}}_k\mathbf{\Gamma}_k^T$ and $\mathbf{P}_{k+1} = (\mathbf{I} - \mathbf{K}_{k+1}\mathbf{C}_{k+1})\mathbf{P}_{k+1}^-$.

The judgment condition for the divergence of the AEKF algorithm is defined as

$$\tilde{\mathbf{Y}}_{k+1}^T\tilde{\mathbf{Y}}_{k+1} \le r\mathrm{Tr}\left(E\left(\tilde{\mathbf{Y}}_{k+1}^T\tilde{\mathbf{Y}}_{k+1}\right)\right) \tag{27}$$

where r is the adjustable coefficient, and $r \ge 1$; different r is selected, corresponding to different systems. Tr is the trace of the matrix.

If (27) is not true, then the filter may be divergent, and the priori values are not accurate.

2) SOC Estimation With AEKF: Transform (1) to a discrete system

$$\begin{cases} U_{\mathrm{pa},k} = U_{\mathrm{pa},k-1}\exp\left(-\Delta t/(R_{\mathrm{pa}}C_{\mathrm{pa}})\right) \\ \qquad + i_{L,k-1}R_{\mathrm{pa}}\left(1 - \exp\left(-\Delta t/(R_{\mathrm{pa}}C_{\mathrm{pa}})\right)\right) \\ U_{\mathrm{pc},k} = U_{\mathrm{pc},k-1}\exp\left(-\Delta t/(R_{\mathrm{pc}}C_{\mathrm{pc}})\right) \\ \qquad + i_{L,k-1}R_{\mathrm{pc}}\left(1 - \exp\left(-\Delta t/(R_{\mathrm{pc}}C_{\mathrm{pc}})\right)\right) \\ U_{L,k} = U_{\mathrm{OC}}(s_k) - i_{L,k}R_O - U_{\mathrm{pa},k} - U_{\mathrm{pc},k}. \end{cases} \tag{28}$$

In contrast with (20), the expressions of matrixes and vectors are listed as follows:

$$\mathbf{X} = \begin{pmatrix} U_{\mathrm{pa}} \\ U_{\mathrm{pc}} \\ s \end{pmatrix}$$

$$\mathbf{A}_{k-1} = \begin{pmatrix} \exp(-\Delta t/(R_{\mathrm{pa}}C_{\mathrm{pa}})) & 0 & 0 \\ 0 & \exp(-\Delta t/(R_{\mathrm{pc}}C_{\mathrm{pc}})) & 0 \\ 0 & 0 & 1 \end{pmatrix}$$

$$\mathbf{B}_{k-1} = \begin{pmatrix} R_{\mathrm{pa}}\left(1 - \exp\left(-\Delta t/(R_{\mathrm{pa}}C_{\mathrm{pa}})\right)\right) \\ R_{\mathrm{pc}}\left(1 - \exp\left(-\Delta t/(R_{\mathrm{pc}}C_{\mathrm{pc}})\right)\right) \\ \eta\Delta t/C_N \end{pmatrix}$$

$$\mathbf{C}_{k-1} = \left.\frac{\partial \mathbf{U}_L}{\partial \mathbf{X}}\right|_{\mathbf{X}=\hat{\mathbf{X}}_{k-1}} = \begin{bmatrix} -1 & -1 & \frac{dU_{\mathrm{OC}}(s)}{ds} \end{bmatrix}$$

$$\mathbf{D} = [R_O].$$

The charging/discharging current is loaded on the lithium-ion battery module and the battery model simultaneously. The

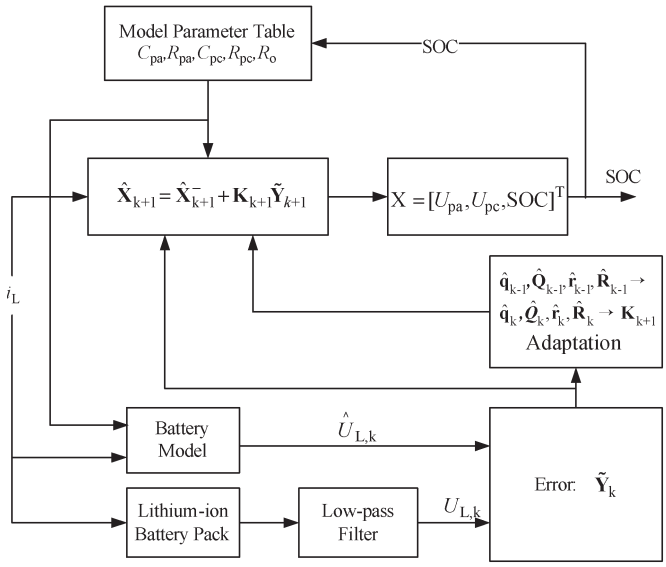

Fig. 10. SOC estimation method based on AEKF.

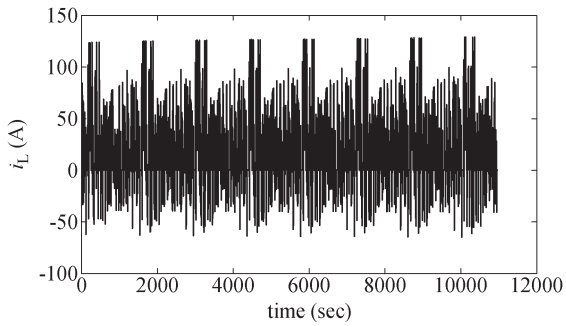

Fig. 11. Current profile sampled during eight consecutive FUDS cycles.

voltage error between the estimation and the experimental data is reduced by adaptively updating the AEKF observer gain. Then, the observer with the updated gain is used to compensate for the state estimation error. The SOC is determined by the estimated voltage based on the open-circuit voltage profile of the battery module. The estimation of SOC is then fed back to update the parameters of the battery module model for the next SOC estimation. In addition, the SOC estimation method based on AEKF is shown in Fig. 10.

C. Verification and Evaluation

The federal urban driving schedules (FUDS) is a typical driving cycle that is often used to evaluate various SOC estimation algorithms [17], [27]–[29]. For Digatron EVT500-500, the FUDS test is an existing program, and BTS-600 uses the TABLE operator to run the FUDS test, which is normally terminated by a certain amount of ampere hours removed from the battery or if the battery reaches a certain voltage level. In this paper, eight periods of FUDS are employed to verify the SOC estimation approach. The current profiles sampled during eight consecutive FUDS cycles are shown in Fig. 11.

TABLE IV
STATISTIC LIST OF THE VOLTAGE ERRORS WITH EKF AND AEKF

	Maximum	Mean	Variance	Error rate
EKF	1.285 V	0.0451 V	0.1204 V^2	2.67%
AEKF	0.605 V	0.0129 V	0.0125 V^2	1.26%

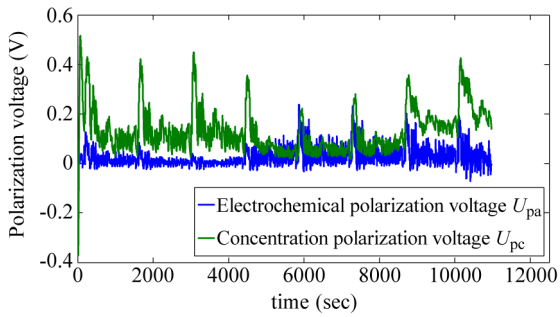

Fig. 12. Polarization voltage curve of lithium-ion battery module.

For the lithium-ion battery module, the initial parameters for the AEKF are specified as follows:

$$\mathbf{A}_1 = \mathbf{A}_0 = \begin{bmatrix} 148 & 0 & 0 \\ 0 & 1.001 & 0 \\ 0 & 0 & 1 \end{bmatrix}$$

$$\mathbf{B}_1 = \mathbf{B}_0 = \begin{bmatrix} -0.1474 & 0 & 0 \\ 0 & -0.0001 & 0 \\ 0 & 0 & 0.01 \end{bmatrix}$$

$$\mathbf{C}_1 = \mathbf{C}_0 = [-1 \quad -1 \quad -4]^T$$

$$\mathbf{D}_1 = \mathbf{D}_0 = [0.02225]$$

$$\mathbf{\Gamma} = \begin{bmatrix} 1 & 0 & 0 \\ 0 & 1 & 0 \\ 0 & 0 & 1 \end{bmatrix}$$

$$\mathbf{P}_0 = \begin{bmatrix} 10 & 0 & 0 \\ 0 & 10 & 0 \\ 0 & 0 & 0.1 \end{bmatrix}$$

$$\hat{\mathbf{Q}}_0 = \begin{bmatrix} 0.001 & 0 & 0 \\ 0 & 0.001 & 0 \\ 0 & 0 & 0.001 \end{bmatrix}.$$

The AEKF algorithm can precisely estimate the voltage and timely modulate the noise signal according to the error matrix. The comparison between the EKF and the AEKF is summarized in Table IV.

Fig. 12 presents the instantaneous polarization voltage curves, which also represent the dynamic performance of the improved Thevenin model and objectively simulate the polarization characteristics of the lithium-ion battery module.

In terms of the AEKF, the electrochemical polarization voltage gradually increases when the open-circuit voltage decreases under the FUDS cycle, whereas the fluctuation of the concentration polarization voltage will be slowed down tardily. Therefore, it is necessary to separately analyze the electrochemical and concentration polarization voltages, which can greatly improve the accuracy and feasibility of the proposed model and the estimated approach. Figs. 13 and 14 show the comparison

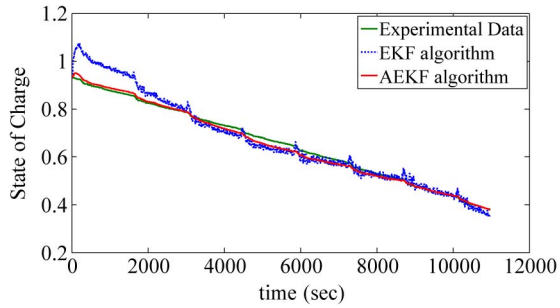

Fig. 13. SOC curves with EKF estimation, AEKF estimation, and experiment.

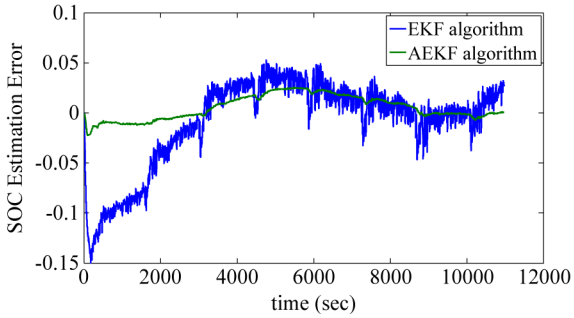

Fig. 14. SOC estimation error curves with EKF and AEKF.

TABLE V
STATISTIC LIST OF SOC ESTIMATION ERROR

	Maximum	Mean	Variance
KEF	14.96%	3.19%	0.001
AKEF	2.54%	1.06%	5.75×10^{-5}

of the SOC curves and its error curves with EKF and AEKF estimations, respectively.

From Figs. 13 and 14, it can be seen that the AEKF presents the improvements in tracking performance and fast convergence, whereas the EKF provides the performance of the slow convergence and instability, which is adverse to the application in EVs. The detailed statistical analysis is shown in Table V.

The AEKF algorithm can compensate the model error and the presetting error of the noise statistics, which has numerical stability and high accuracy. On one hand, the priori error occurs in model parameters and the noise statistics. The noise observer can estimate the mean as well as the covariance of dynamic noise according to the predictive residual $\mathbf{X}_k - (\mathbf{A}_{k-1}\mathbf{X}_{k-1} + \mathbf{B}_{k-1}\mathbf{u}_{k-1})$ and measurement residual $\tilde{\mathbf{Y}}_k$; consequently, the model and the noise statistics error can be compensated. On the other hand, the adaptive algorithm can improve the stability and robustness of the algorithm via real-time online correction. Normally, the Kalman filter algorithm possesses a certain stability; however, it easily causes divergence due to the error existing in the model and the noise statistics, particularly the noise statistics evaluated by the trial-and-error method. Fig. 13 shows that the divergence took place using the EKF algorithm at the earlier stage of the SOC estimation, and the estimation error reached 14.96%. Nevertheless, the remarkable merit of the AEKF algorithm is the real-time amendment. Although the maximum absolute error of the AEKF algorithm is 2.54%, the absolute error mean is only 1.06%, and the error variance is very small, which manifests its fast convergence, stability, and minor error. Thus, the proposed approach of the SOC estimation algorithm is suitable for a lithium-ion power battery module, which can quickly reduce the model error and improve the accuracy of the filter.

IV. CONCLUSION

For a lithium-ion battery module, an improved Thevenin model has been proposed, and its parameter identification is performed using the EKF algorithm. The experimental and simulation results show that the maximum error of the improved Thevenin model is within 4.15%, and the error covariance is 0.0708 V^2. The proposed model has achieved enough accuracy.

To improve the accuracy, reliability, and robustness of the SOC estimation, an SOC estimation with AEKF algorithm was put forward based on the improved Thevenin model. After eight FUDS cycles, the maximum error of the SOC estimation is within 2.54%, and its mean is only 1.06%, which present that the estimation algorithm has higher accuracy compared with the EKF algorithm.

ACKNOWLEDGMENT

The authors would like to thank Dr. Z. Cai-Ping of Beijing Jiaotong University for many helpful discussions and data support.

REFERENCES

[1] B. Mashadi and S. A. M. Emadi, "Dual-mode power-split transmission for hybrid electric vehicles," *IEEE Trans. Veh. Technol.*, vol. 59, no. 7, pp. 3223–3232, Sep. 2010.
[2] Q. M. Gong, Y. Y. Li, and Z. R. Peng, "Trip-based optimal power management of plug-in hybrid electric vehicles," *IEEE Trans. Veh. Technol.*, vol. 57, no. 6, pp. 3393–3401, Nov. 2008.
[3] H. Hongwen, Y. Song, and X. Zhenjun, "Integrated control method for a fuel cell hybrid system," *Asia-Pac. J. Chem. Eng.*, vol. 4, no. 1, pp. 68–72, Jan./Feb. 2009.
[4] N. L. Chaturvedi, R. Klein, J. Christensen, J. Ahmed, and A. Kojic, "Algorithms for advanced battery-management systems," *IEEE Control Syst. Mag.*, vol. 30, no. 3, pp. 49–68, Jun. 2010.
[5] D. Y. Jung, B. H. Lee, and S. W. Kim, "Development of battery management system for nickel-metal hydride batteries in electric vehicle applications," *J. Power Sources*, vol. 109, no. 1, pp. 1–10, Jun. 2002.
[6] D. T. Lee, S. J. Shiah, C. M. Lee, and Y. C. Wang, "State-of-charge estimation for electric scooters by using learning mechanisms," *IEEE Trans. Veh. Technol.*, vol. 56, no. 2, pp. 544–556, Mar. 2007.
[7] J. Alzieu, H. Smimite, and C. Glaize, "Development of an on-board charge and discharge management system for electric-vehicle batteries," *J. Power Sources*, vol. 53, no. 2, pp. 327–333, Feb. 1995.
[8] I. Snihir, W. Rey, E. Verbitskiy, A. Belfadhel-Ayeb, and P. H. L. Notten, "Battery open-circuit voltage estimation by a method of statistical analysis," *J. Power Sources*, vol. 159, no. 2, pp. 1484–1487, Sep. 2006.
[9] J. C. Peng, Y. B. Chen, and R. Eberhart, "Battery pack state of charge estimator design using computational intelligence approaches," in *Proc. 15th Annu. Battery Conf. Appl. Adv.*, Long Beach, CA, 2000, pp. 173–177.
[10] A. Szumanowski and Y. H. Chang, "Battery management system based on battery nonlinear dynamics modeling," *IEEE Trans. Veh. Technol.*, vol. 57, no. 3, pp. 1425–1432, May 2008.
[11] P. J. V. Bree, A. Veltman, W. H. A. Hendrix, and P. P. J. V. D. Bosch, "Prediction of battery behavior subject to high-rate partial state of charge," *IEEE Trans. Veh. Technol.*, vol. 58, no. 2, pp. 588–595, Feb. 2009.
[12] G. L. Plett, "Extended Kalman filtering for battery management systems of LiPB-based HEV battery packs—Part 3. State and parameter estimation," *J. Power Sources*, vol. 134, no. 2, pp. 277–292, Aug. 2004.

[13] J. Lee, O. Nam, and B. H. Cho, "Li-ion battery SOC estimation method based on the reduced order extended Kalman filtering," *J. Power Sources*, vol. 174, no. 1, pp. 9–15, Nov. 2007.
[14] J. Han, D. Kim, and M. Sunwoo, "State-of-charge estimation of lead-acid batteries using an adaptive extended Kalman filter," *J. Power Sources*, vol. 188, no. 2, pp. 606–612, Mar. 2009.
[15] A. Vasebi, M. Partovibakhsh, and S. Bathaee, "A novel combined battery model for state-of-charge estimation in lead-acid batteries based on extended Kalman filter for hybrid electric vehicle applications," *J. Power Sources*, vol. 174, no. 1, pp. 30–40, Nov. 2007.
[16] P. Shi, Y. W. Zhao, and P. Shi, "Application of unscented Kalman filter in the SOC estimation of Li-ion battery for Autonomous Mobile Robot," in *Proc. IEEE Int. Conf. Inf. Acquisition*, Weihai, China, 2006, pp. 1279–1283.
[17] G. L. Plett, "Sigma-point Kalman filtering for battery management systems of LiPB-based HEV battery packs—Part 1: Introduction and state estimation power sources," *J. Power Sources*, vol. 161, no. 2, pp. 1356–1368, Oct. 2006.
[18] S. Dan, *Optimal State Estimation: Kalman, H and Nonlinear Approaches*. New York: Wiley-Interscience, 2006.
[19] D. V. Do, C. Forgez, K. E. K. Benkara, G. Friedrich, and Guy, "Impedance observer for a Li-ion battery using Kalman filter," *IEEE Trans. Veh. Technol.*, vol. 58, no. 8, pp. 3930–3937, Oct. 2009.
[20] S. J. Julier and J. K. Uhlmann, "Unscented filtering and nonlinear estimation," *Proc. IEEE*, vol. 92, no. 3, pp. 401–422, Mar. 2004.
[21] G. Welch and G. Bishop, "An introduction to the Kalman filter," in *Proc. SIGGRAPH*, Los Angeles, CA, 2001.
[22] Q.-H. Meng, Y. C. Sun, and Z. L. Cao, "Adaptive extended Kalman filter (AEKF)-based mobile robot localization using sonar," *Robotica*, vol. 18, no. 5, pp. 459–473, Sep. 2000.
[23] V. H. Johnson, "Battery performance models in ADVISOR," *J. Power Sources*, vol. 110, no. 2, pp. 321–329, Aug. 2002.
[24] *Battery Application Manual*, Gates Energy Products, Inc., Gainesville, FL, 1989.
[25] *PNGV Battery Test Manual*, INEEL, Idaho Falls, ID, 2001. [Online]. Available: http://avt.inel.gov/battery/pdf/pngv_manual_rev3b.pdf
[26] A. P. Sage and G. W. Husa, "Adaptive filtering with unknown prior statistics," in *Proc. Joint Amer. Control Conf.*, 1969, pp. 769–774.
[27] J. P. Wang, Q. S. Chen, and B. G. Cao, "Support vector machine based battery model for electric vehicles," *Energy Convers. Manage.*, vol. 47, no. 7/8, pp. 858–864, May 2006.
[28] J. P. Wen, J. C. Jiang, F. Wen, and W. G. Zhang, "Source error analysis of Kalman algorithm in its application to SOC estimation in PEV," *Qiche Gongcheng/Automotive Eng.*, vol. 32, no. 3, pp. 188–192, 227, 2010.
[29] C. T. Lin, Q. S. Chen, J. P. Wang, W. H. Huang, and Y. C. Wang, "Improved Ah counting method for state of charge estimation of electric vehicle batteries," *J. Tsinghua Univ. Sci. Technol.*, vol. 46, no. 2, pp. 247–251, 2006.

Hongwen He received the M.E. degree in vehicle engineering from the Jilin University of Technology, Changchun, China, in 2000 and the Ph.D. degree in vehicle engineering from the Beijing Institute of Technology, Beijing, China, in 2003.

He is currently an Associate Professor with the National Engineering Laboratory for Electric Vehicles, School of Mechanical Engineering, Beijing Institute of Technology. He has published more than 60 papers and holds six patents. His research interests include power battery modeling and simulation, electric vehicles, design, and control theory of the hybrid power train.

Dr. He received the first prize of Scientific or Technical Awards from the Beijing Institute of Technology in 2007.

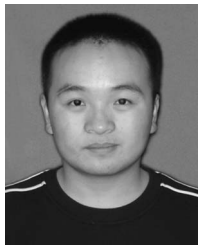

Rui Xiong received the M.E. degree in vehicle engineering in 2010 from the Beijing Institute of Technology, Beijing, China, where he is currently working toward the Ph.D. degree in vehicle engineering.

He has published seven papers. His research mainly focuses on modeling and simulation, power batteries, and vehicular hybrid power systems.

Xiaowei Zhang received the M.E. degree in 2007 from the Beijing Institute of Technology, Beijing, China, where he is currently working toward the Ph.D. degree in vehicle engineering.

He has published three papers. His research mainly focuses on optimization control and hardware-in-the-loop (HIL) simulation of the vehicular hybrid power train.

Fengchun Sun received the M.E. and Ph.D. degrees in vehicle engineering from the Beijing Institute of Technology, Beijing, China, in 1984 and 1989, respectively. He studied at the Technical University of Berlin, Berlin, Germany, from 1987 to 1989 as a joint Ph.D. degree student.

He is currently a Professor and the Vice President of the Beijing Institute of Technology and the Director of the National Engineering Laboratory for Electric Vehicles. He has been conferred the title of "Cheung Kong Scholar" by the Ministry of Education, China. He has published more than 150 papers and is the holder of 19 patents. His research interests include electric vehicles, electric drive systems, electric vehicle demonstration, and infrastructure.

Dr. Sun received the second prize from the National Science and Technology Progress Awards in 2008, the second prize from the National Technological Innovation Awards in 2004 and 2009, and the award for industrial innovation from the Ho Leung Ho Lee Foundation in 2007.

JinXin Fan (S'10) received the M.E. degree in vehicle engineering from Anhui Agricultural University, Hefei, China, in 2004. She is currently working toward the Ph.D. degree in vehicle engineering with the National Engineering Laboratory for Electric Vehicles, Beijing Institute of Technology, Beijing, China. She studied at Michigan State University, East Lansing, from 2008 to 2010, as a joint Ph.D. degree student.

Her research mainly focuses on permanent-magnet electric machines, cooling systems, and thermal analysis, particularly in the field of electric vehicles.